

# X-ray shadows of the Draco nebula

## A new method to determine total hydrogen column densities

P. Moritz<sup>1</sup>, A. Wennmacher<sup>1,2</sup>, U. Herbstmeier<sup>1,3</sup>, U. Mebold<sup>1</sup>, R. Egger<sup>4</sup>, and S.L. Snowden<sup>4,5</sup>

<sup>1</sup> Radioastronomisches Institut der Universität Bonn, Auf dem Hügel 71, D-53121 Bonn, Germany

<sup>2</sup> Institut für Geophysik und Meteorologie, Universität zu Köln, Albertus-Magnus-Platz, D-50923 Köln, Germany

<sup>3</sup> Max-Planck-Institut für Astronomie, Königstuhl 17, D-69117 Heidelberg, Germany

<sup>4</sup> Max-Planck-Institut für Extraterrestrische Physik, D-85740 Garching, Germany

<sup>5</sup> NASA/Goddard Space Flight Center, M/C 685, Greenbelt, MD 20771, USA

Received 5 August 1997 / Accepted 8 April 1998

**Abstract.** We have used the ROSAT  $\frac{1}{4}$  keV all-sky survey together with H I observations to derive the total column density of hydrogen nuclei,  $N(\text{H})$ , of the Draco nebula [= G91+38 ( $v_{\text{LSR}} = -21 \text{ km s}^{-1}$ )], which casts a deep shadow in the soft X-ray background. Adopting a two-component model for the X-ray plasma in which one component is located behind the Draco nebula, the other in front of all the absorbing material (the so-called Local Hot Bubble, LHB), we fit the parameters of the radiation transport equation to the observed X-ray count rates. The optical depth in this equation is derived from H I column densities obtained with the 100-m telescope and the appropriate X-ray absorption cross sections. The solutions obtained by this approach are biased since H I column densities underestimate the absorption in regions where molecular hydrogen is abundant. The bias is avoided by excluding regions with strong X-ray shadowing from the fit and by comparing fits which are obtained on the basis of hydrogen column densities derived from IRAS 100  $\mu\text{m}$  data.

We find that the absorbing column densities at the deepest X-ray shadows are up to about  $3 \cdot 10^{20} \text{ cm}^{-2}$  larger than the observed H I column densities. At the edge towards low galactic latitudes and longitudes, up to 70% of the hydrogen is in molecular form. In other parts of the nebula the molecular abundance is  $\lesssim 25\%$ .

We also find an approximately constant FIR-emissivity per hydrogen nucleon ( $\text{H I} + 2\text{H}_2$ ) of about  $1.0 \cdot 10^{-20} \text{ MJy sr}^{-1} \text{ cm}^2$ . This is close to the mean value for the galactic cirrus ( $0.86 \cdot 10^{-20} \text{ MJy sr}^{-1} \text{ cm}^2$ ). In contrast, the FIR-emissivity per H I atom is varying strongly across the nebula.

The  $x_{\text{WCO}}$  values ( $\equiv N(\text{H}_2)/W(^{12}\text{CO})$ ) found in the Draco nebula are typically in the range  $0.34 < x_{\text{WCO}} < 0.52 \cdot 10^{20} \text{ cm}^{-2} (\text{K km s}^{-1})^{-1}$ , similar to other cirrus clouds. We find a very low  $x_{\text{WCO}}$  ratio of  $0.17 \text{ cm}^{-2} (\text{K km s}^{-1})^{-1}$  at the edge of the Draco nebula towards low galactic coordinates where the CO abundance could be altered in a low-velocity shock.

Finally, the X-ray emission measure for the distant component of the X-ray emitting plasma is found to be about 5 times larger than that for the LHB, assuming constant plasma temperatures of  $10^{6.3} \text{ K}$  and  $10^{5.85} \text{ K}$  respectively. Since the Draco nebula (distance  $> 300 \text{ pc}$ ) is located outside the galactic gas layer, this is evidence of a bright Galactic X-ray corona or an extended coronal hot spot. The intensity of this coronal emission is constant over the observed  $7^\circ$ -field within the uncertainties of our analysis ( $< 15\%$ ).

**Key words:** ISM: atoms – ISM: clouds – dust, extinction – ISM: individual objects: Draco nebula – ISM: molecules – X-rays: ISM

### 1. Introduction

The determination of total hydrogen column density,  $N(\text{H})$ , plays an important role in studies of the structure and the evolution of galaxies. This value controls quantities like the total mass, extinction, and density of interstellar clouds or cloud complexes. For molecular clouds, estimates of  $N(\text{H})$  are complicated as direct measurements of the column densities of molecular hydrogen,  $N(\text{H}_2)$ , are only feasible for selected small-scale regions, via far-ultraviolet or near-infrared absorption line analyses toward strong continuum sources.

Frequently used secondary tracers for total hydrogen column densities are diffuse galactic  $\gamma$ -rays (see e.g. Strong et al. 1988) and the diffuse infrared emission at 100  $\mu\text{m}$  wavelength. Their calibration by the observed atomic neutral hydrogen column density,  $N(\text{H I})$ , gives the emission per hydrogen nucleus of  $\gamma$ - and 100  $\mu\text{m}$  radiation. The velocity-integrated intensity of the  $J = 1 \rightarrow 0$  transition of  $^{12}\text{CO}$  at 2.6 mm,  $W(^{12}\text{CO})$ , is also used as a tracer of molecular hydrogen. Applying a conversion factor between the observed  $^{12}\text{CO}$  line intensity and the  $\text{H}_2$  column density,  $x_{\text{WCO}} \equiv N(\text{H}_2)/W(^{12}\text{CO})$ , gives  $N(\text{H}_2)$  if  $W(^{12}\text{CO})$  has been measured. Analyses near the galactic plane suggest an average  $x_{\text{WCO}}$  factor between  $1.6 \cdot 10^{20} \text{ cm}^{-2} (\text{K km s}^{-1})^{-1}$  and  $2.3 \cdot 10^{20} \text{ cm}^{-2} (\text{K km s}^{-1})^{-1}$  (Strong et al. 1988, Bloemen

et al. 1990). For diffuse and translucent clouds of the galactic cirrus, de Vries et al. (1987) have determined an  $x_{WCO}$  factor of about  $0.5 \cdot 10^{20} \text{ cm}^{-2} (\text{K km s}^{-1})^{-1}$ . Similar values have been found by Heithausen & Mebold (1989), Meyerdierks et al. (1990) and Heithausen & Thaddeus (1990) for other high latitude clouds. Herbstmeier et al. (1993) even found values in the range  $0.02 \cdot 10^{20} < x_{WCO} < 0.26 \cdot 10^{20} \text{ cm}^{-2} (\text{K km s}^{-1})^{-1}$ . These large quantitative differences between different regions of the Galaxy or even within one molecular cloud complex show that the appropriate conversion factor depends on the physical and chemical state of the cloud observed and the conditions imposed by the environment. Meyerdierks & Heithausen (1996) even found a large-scale infrared excess in the direction of the Polaris Flare, without corresponding CO emission, which they interpret as evidence for diffuse molecular hydrogen. A method to determine the  $\text{H}_2$  content of interstellar clouds independent of CO emission is therefore highly warranted.

A direct way to derive the total hydrogen column density of galactic clouds can be achieved on the basis of soft X-ray observations. If such a cloud is located in front of a bright emission region of the soft X-ray background (SXRb), it is visible as an X-ray shadow. Once the intensity of the X-ray source is known, the  $N(\text{H})$  distribution can be obtained from the analysis of the depth distribution of such a shadow.

In this paper we use the ROSAT  $\frac{1}{4}$  keV survey (see Sect. 2.1) together with 21 cm observations performed with the Effelsberg 100-m telescope (Sect. 2.2) to derive the  $N(\text{H})$  and the  $N(\text{H}_2)$  distribution of the Draco nebula (also called IVC G 091.0+38.0,  $v_{\text{LSR}} = -21 \text{ km s}^{-1}$ , IVC 91+38-21; LBN 406, 412, 415; MBM 41, 42, 43, 44; and G 90.0+38.8, G 94.8+37.6), a molecular cloud with a distance from the galactic plane of  $z > 180 \text{ pc}$  (Lilienthal et al. 1991).

The Draco nebula is a useful object to perform such studies. Deep X-ray shadows in the ROSAT  $\frac{1}{4}$  keV diffuse background cast by two parts of the Draco nebula (Snowden et al. 1991, Burrows & Mendenhall 1991) give evidence of a bright ( $\simeq 10^6 \text{ K}$ ) X-ray corona of the Galaxy in this direction. Furthermore, Herbstmeier et al. (1993; hereafter HHM) have compared the IRAS  $100 \mu\text{m}$  intensity,  $I_{100}$ , of the Draco nebula together with  $N(\text{H I})$  and  $W(^{12}\text{CO})$  and derived  $x_{WCO}$  ratios (simultaneously they determined FIR-emissivities) which are presently the lowest known in the Galaxy (see above). An independent confirmation of their results is therefore important for understanding the physical and chemical processes in high latitude molecular clouds.

We approximate the soft X-ray background by a two-component emission model (see Sect. 3.1) where one component comprises galactic halo and extragalactic emission which are attenuated by the Draco nebula and other absorption structures in the line of sight (Sect. 2.2.1) and one local unabsorbed X-ray source associated with the Local Hot Bubble (LHB, see e.g. Snowden et al. 1990). We fit the two-component model to the observed X-ray count rate distribution (Sect. 3.2) in regions outside the Draco nebula where no molecular hydrogen is expected. The absorbing medium is given by the observed  $\text{H I}$  column density and appropriate absorption cross sections

(Sect. 3.1). This allows the derivation of the intensities of the distant X-ray source and of the LHB and, with certain assumptions, the corresponding emission measures (Sect. 4.1). We show that at several positions on the Draco nebula, the observed X-ray count rates are lower than expected with atomic gas as the only absorber. This deeper shadow is due to an excess absorbing column density,  $N_{exc}$ , associated with molecular gas of the Draco nebula (Sect. 4.2). Special care is taken in checking the homogeneity of the X-ray background because unmodeled variations in the X-ray emission can also produce deviations in the fitted parameters.

We compare the derived total hydrogen column densities,  $N(\text{H}) \equiv N(\text{H I}) + N_{exc}$ , with  $I_{100}$  (see Sect. 2.3) to derive the FIR-emissivity of the Draco nebula (Sect. 4.3) and estimate the  $x_{WCO}$  factor in regions where  $W(^{12}\text{CO})$  has been observed (Sect. 4.4). This allows a direct comparison of our method with that presented by HHM. Finally, the mass and extinction of the Draco nebula are determined (Sect. 4.5).

An independent way to estimate the total hydrogen content of the Draco nebula is to directly correlate the ROSAT  $\frac{1}{4}$  keV survey with  $I_{100}$  (Sect. 5). This is possible since the FIR-intensity appears to be a good measure for the total hydrogen column density. Here the FIR-emissivity is derived simultaneously with the intensities of the foreground and background X-ray components. We compare the results to those obtained in Sect. 4 and discuss the pros and cons of this method. Some conclusions are drawn in Sect. 6.

## 2. The observations

### 2.1. The ROSAT observations

Our X-ray observations are part of the ROSAT (Röntgen Satellite; Trümper 1983,92) all-sky survey (Snowden & Schmitt 1990, Voges 1992, Snowden et al. 1995,97) performed with the XRT (X-Ray Telescope; Aschenbach 1988) during the second half of 1990. For the XRT all-sky survey, only the Position Sensitive Proportional Counter (PSPC, Pfeffermann 1987) was used. The all-sky survey was performed in such a way that one great circle perpendicular to the current position of the Sun in the ecliptic was scanned on the sky each orbit. The plane of the great circle was rotated by  $4'$  each orbit around the ecliptic poles. Since the Draco nebula is located not far away from the north ecliptic pole the cumulative vignetting-corrected exposure for all parts of our region was larger than about 1500 seconds.

The data were derived from photon-event files and ancillary data provided by the Standard Analysis Software System (SASS, Voges et al. 1992). Due to the relatively limited spectral resolution of the PSPC ( $E/\Delta E \sim 1$  at  $\frac{1}{4}$  keV) the photon events were binned into a limited number of broad pulse-height or energy bands. These bands are defined in terms of pulse-height-invariant (PI) channels (Snowden et al. 1994a). Our data were processed in two pulse-height bands: the R1-band (PI channels 8 to 19) and the R2-band (channels 20 to 41). The R1- and R2-band data were combined to produce the  $\frac{1}{4}$  keV band image ( $\simeq 0.08 - 0.284 \text{ keV}$ ) analysed in this paper. The response function of the  $\frac{1}{4}$  keV band as well as the procedure of the image

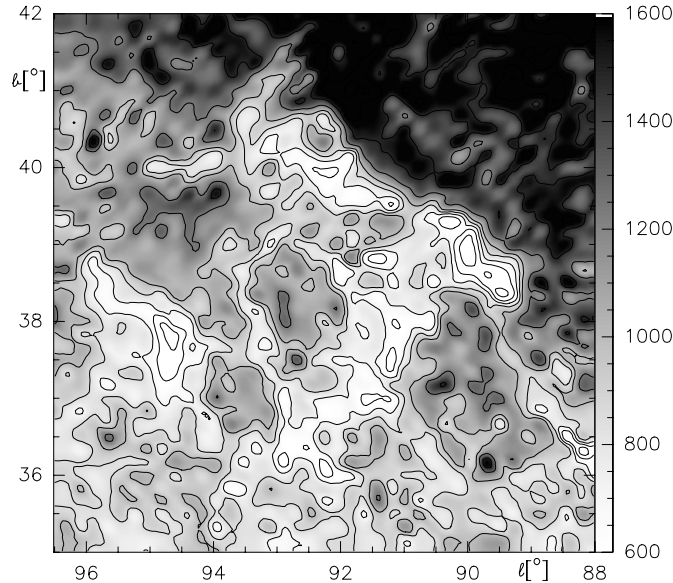


**Fig. 1.** ROSAT  $\frac{1}{4}$  keV all-sky survey of the Draco nebula region. Contours are plotted from 400 to 1000  $10^{-6}$  counts  $s^{-1}$  arcmin $^{-2}$  in steps of 150  $10^{-6}$  counts  $s^{-1}$  arcmin $^{-2}$  and from 1250 to 1750  $10^{-6}$  counts  $s^{-1}$  arcmin $^{-2}$  in steps of 250  $10^{-6}$  counts  $s^{-1}$  arcmin $^{-2}$ . Dark corresponds to large intensities, white to low ones.

construction from the photon-event files are similar to the ones described by Snowden et al. (1994b).

The data have been corrected for the particle background (Snowden et al. 1992; Plucinsky et al. 1993) as well as for scattered solar X-rays (Snowden & Freyberg 1993). The less well understood “long-term enhancements” have also been removed using an empirical model. Its rate was determined by using the redundancy of the ROSAT geometry (Snowden et al. 1995). These enhancements appear primarily in the  $\frac{1}{4}$  keV band, are approximately uniform around an orbit, last about 20-30 orbits, and have peak intensities occasionally comparable to the diffuse X-ray background in the  $\frac{1}{4}$  keV band. In addition, point sources have been removed down to a limiting flux of about 0.02 counts  $s^{-1}$  using masks created from the source list derived from the all-sky survey.

The map of the final count rate distribution of the region of the Draco nebula is shown in Fig. 1. The image has a resolution of  $9.6'$ . The relative statistical count rate uncertainty is between 5 and 18%.

## 2.2. The H I observations

The 21-cm line spectra have been obtained with the 100-m telescope of the Max-Planck-Institut für Radioastronomie at Effelsberg during several observing periods between 1977 and 1993. These observations are fully described by Herbstmeier et al. (1996). All measurements have been calibrated using the IAU standard position S7 and have been corrected for stray radiation (Kalberla et al. 1980, 1982). Baseline corrections have been performed using the method described in Wennmacher (1994).

### 2.2.1. H I structure in the region of the Draco nebula

In the region of the Draco nebula, H I emission is found at various velocities in the range  $-210$  to  $+15$  km  $s^{-1}$ . The corresponding H I channel maps of the mean brightness temperature are presented by Herbstmeier et al. (1996). Towards the high latitude part of our figures and towards the center region of the Draco nebula at  $(l, b) = (91.5^\circ, 38.5^\circ)$  filamentary and clumpy high-velocity clouds (HVCs) are visible having centre velocities of  $-120$  km  $s^{-1}$  and  $-140$  km  $s^{-1}$ , respectively. They belong to the HVC Complex C described e.g. by Wakker (1991). So-called intermediate velocity clouds (IVCs) are mainly seen at galactic longitudes  $l > 94^\circ$ . The bulk of this H I emission is found at velocities between  $-50$  and  $-30$  km  $s^{-1}$ . These clouds are probably related to the nearby IVC loop GS 155 + 38 – 58 (Heiles 1984). The Draco nebula filaments show up at velocities in the range  $-30$  to  $-10$  km  $s^{-1}$ . The distance of the Draco nebula is larger than 300 pc and has a most probable value at about 600 pc (see Lilienthal et al. and references therein). The emission at low velocities is dominated by the diffuse warm interstellar medium. This component is seen all over the whole region and decreases towards higher latitudes. Wennmacher (1994) has determined its mean distance to 290 pc. Furthermore, towards low galactic coordinates the emission of the cold dense filament LVC 88 + 36 – 2 is visible which has a mean distance of only about 60 pc. This filament is discussed in detail by Wennmacher (1994).

To separate the emission of the Draco nebula from the other cloud structures, the spectra have been decomposed into gaussian components by a method described by Haud (1993). A component is associated with the Draco nebula if the centre velocity is in the range between  $-30$  and  $-13$  km  $s^{-1}$ , and if the velocity dispersion is smaller than  $7$  km  $s^{-1}$  as described in HHM. The H I column density of each component is calculated assuming that the 21-cm line is optically thin. Fig. 2 shows the map of the total H I column density in the velocity range  $-50$  to  $+15$  km  $s^{-1}$  which does contain all features described in the last paragraph except the HVCs. It has an uncertainty of about  $2 \cdot 10^{19}$  cm $^{-2}$ . The H I column density of the Draco nebula alone is shown in Fig. 6. Its uncertainty is about  $3 \cdot 10^{19}$  cm $^{-2}$ . The maps have the same projection and pixel size as Fig. 1 and are smoothed to the resolution of the X-ray data.

## 2.3. The IRAS observations

The IRAS measurements of the Draco nebula have already been presented by Odenwald & Rickard (1987) and by HHM. Here we use the same 100  $\mu$ m data set as described by the latter authors. The 100  $\mu$ m IRAS Sky Flux image has been corrected for scanning effects using a procedure of van Albada et al. (1984) at Groningen (NL). The resolution of the 100  $\mu$ m maps is  $3' \times 5'$  in equatorial coordinates. The data have been smoothed and reprojected to the resolution and pixel size of the X-ray data. We have subtracted the emission of the zodiacal dust which contributes to the FIR-intensity with  $I_{100,Z} = 2.15 / \sin \beta$  (Boulanger & Pérault 1988) where  $\beta$  is the ecliptic latitude.

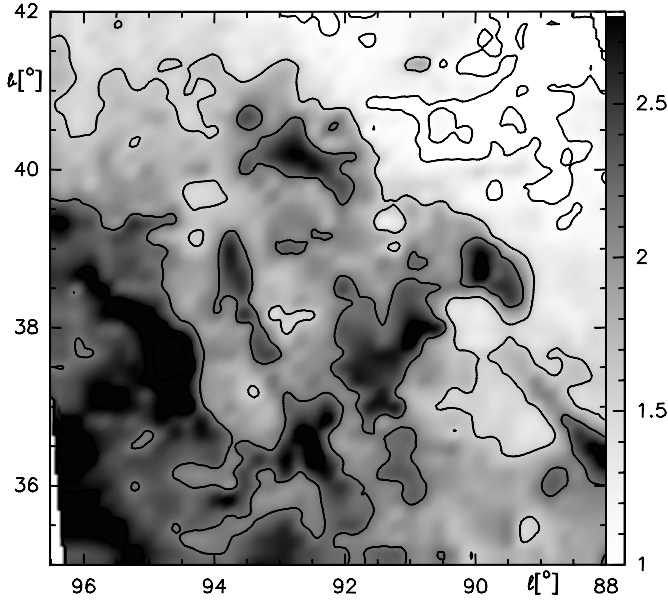


**Fig. 2.** Total H I column density of the region of the Draco nebula in the velocity range  $-50 < v_{\text{LSR}} < 15 \text{ km s}^{-1}$ . Contours are plotted at 1.0, 1.6, 2.2, 2.8 and  $3.4 \cdot 10^{20} \text{ atoms cm}^{-2}$ . Dark corresponds to large intensities, white to low ones.

The  $100 \mu\text{m}$  intensity,  $I_{100}$ , is used as a measure of the sum of the atomic and the molecular neutral hydrogen column densities,  $N_{\text{H}}$ . However, there are strong indications that the FIR-emissivity per hydrogen nucleon of the dust associated with the Draco nebula differs from that of the dust associated with the diffuse H I layer (see HHM). We take this into account by treating the contributions of the diffuse gas and the Draco nebula separately.

Regions outside the Draco nebula and other local cloud structures (see Sect. 2.2) show only the FIR-emission of the diffuse H I layer. We use the observed column densities in these regions and find

$$\begin{aligned} I_{100,\text{BG}} &= a_{100,\text{BG}} N(\text{H I})_{\text{BG}} + I_{100,\text{OS}} \\ &= 0.87 \cdot 10^{-20} \text{MJy sr}^{-1} \text{cm}^2 N(\text{H I})_{\text{BG}} \\ &\quad + 1.84 \text{MJy sr}^{-1} \end{aligned} \quad (1)$$

with a correlation coefficient of 0.92. The slope of this relation, the FIR-emissivity of the diffuse H I gas,  $a_{100,\text{BG}}$ , as well as the offset background emission,  $I_{100,\text{OS}}$ , are in good agreement with corresponding values found by Boulanger & Péroul (1988) for the diffuse H I layer. They identify an offset emission of  $(1.8 \pm 0.3) \text{MJy sr}^{-1}$  that they find for the polar caps ( $|b| > 50^\circ$ ) as a combination of extragalactic emission, emission of dust associated with ionized hydrogen, uncertainties of the zero-level calibration of the IRAS data, and deviations of the zodiacal contribution from the cosecant-law.

HHM have shown that the FIR-emission of the Draco nebula can be well separated from the background FIR-emission by fitting a cosecant-law to the total FIR-emission (including zodi-

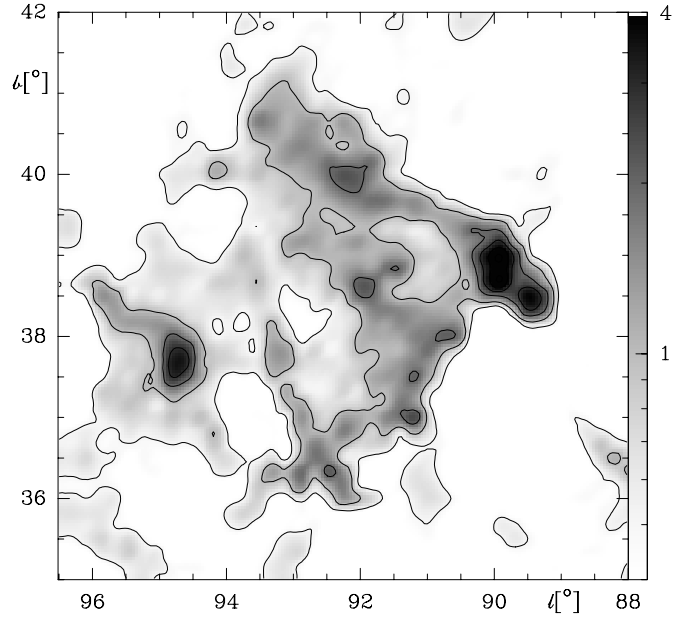


**Fig. 3.** IRAS  $100 \mu\text{m}$  image of the Draco nebula region. Zodiacal dust emission and emission associated with the diffuse galactic H I layer have been subtracted in this image (for details see Sect. 2.3). The contour lines are plotted at 0.5, 1, 2, 3 and  $4 \text{ MJy sr}^{-1}$ . Dark corresponds to large intensities, white to low ones.

acal emission) in regions outside the Draco nebula. The  $100 \mu\text{m}$  emission associated with the Draco nebula is thus given by

$$I_{100,\text{DN}} = I_{100} - \left( \frac{4.17}{\sin b} - \frac{2.15}{\sin \beta} - 1.52 \right) \text{MJy sr}^{-1} \quad (2)$$

The map of the  $100 \mu\text{m}$  distribution of the Draco nebula is shown in Fig. 3.

Combining the above, the total neutral hydrogen column density,  $N(\text{H})$ , as a function of  $I_{100}$ , of the nebula and the diffuse gas in the line of sight is given by

$$N(\text{H}) = \frac{I_{100,\text{DN}}}{a_{100,\text{DN}}} + \frac{I_{100,\text{BG}} - 1.84 \text{MJy sr}^{-1}}{0.87 \cdot 10^{-20} \text{MJy sr}^{-1} \text{cm}^2}, \quad (3)$$

where  $a_{100,\text{DN}}$  is the FIR-emissivity of the dust associated with the Draco nebula. HHM find large variations of this value across the Draco nebula by comparing  $I_{100}$  with H I and CO line emission. The comparison of the ROSAT  $\frac{1}{4} \text{ keV}$  survey with H I allows an independent check of the FIR-emissivities of HHM.

#### 2.4. The CO observations

The Draco nebula has been observed with the POM1 telescope at Bordeaux (Mebold et al. 1985) and the KOSMA 3 m telescope (Mebold et al. 1989) in the  $J=1 \rightarrow 0$  line of the  $^{12}\text{CO}$  molecule. The observational parameters of all these measurements are summarized by HHM. These authors have performed a decomposition of the observed spectra into gaussians to derive the CO line integrals,  $W(^{12}\text{CO})$ . In Sect. 4.4 we compare these values to the molecular hydrogen column densities of the Draco

nebula,  $N(\text{H}_2)$ , obtained from our X-ray and H I data in order to get a new estimate of the conversion factor,  $x_{\text{WCO}}$ .

### 3. The model

#### 3.1. Radiative transfer

The shadow in the soft X-ray count rates at the position of the brightest FIR or H I features of the Draco nebula (shadow depth: 70%) suggests a two-component model to approximate the hot plasma layer along the lines of sight. In this model the observed  $\frac{1}{4}$  keV band count rate in a given direction,  $C_{\text{obs}}$ , is the sum of foreground emission,  $C_{\text{Fg}}$ , and attenuated background emission,  $C_{\text{Bg}}$ :

$$C_{\text{obs}} = C_{\text{Fg}} + C_{\text{Bg}} \exp(-\tau) \quad (4)$$

The foreground component is associated with hot plasma from the Local Hot Bubble (Snowden et al. 1990). The distant component consists of contributions from the galactic halo and truly extragalactic sources (see Hasinger et al. 1993).  $C_{\text{Bg}}$  is attenuated by photoelectric absorption both by the Draco nebula and the galactic H I layer including the clouds observed at velocities larger than  $-50 \text{ km s}^{-1}$ . We neglect the possibility of X-ray emission intermixed with these clouds. The simple two-component model is not valid in the direction of LVC 88+36-2 (see Sect. 2.2) because this filament is located inside the LHB and therefore attenuates also the LHB component (Kerp et al. 1993). The two-component approximation is also questionable in the direction towards the HVC filaments (Sect. 2.2) because these clouds are associated with soft X-ray emission (Kerp et al. 1994). Furthermore, the unknown and probably large distance of these clouds does not permit the assumption that the HVCs are located in front of the halo component. Therefore these regions are avoided in the present model fits.

We assume standard interstellar elemental abundances which are constant along the line of sight and adopt a constant degree of ionization of hydrogen. Then the optical depth is given by

$$\tau = \bar{\sigma}_T(N_{\text{H}}) N_{\text{H}} \quad (5)$$

$N_{\text{H}} = N(\text{H I}) + 2 N(\text{H}_2)$  is the total neutral hydrogen column density in the line of sight.  $\bar{\sigma}$  is the photoelectric absorption cross section averaged for the bandpass observed with the ROSAT PSPC. Because the absorption cross section decreases with increasing photon energy (see Morrison & McCammon 1983) the band-averaged value depends on the absorbing hydrogen column density and on the intrinsic spectrum of the X-ray emission which is mainly a function of the plasma temperature  $T$ . Kerp (1994) has found an approximately constant temperature of  $10^{6.3 \pm 0.1}$  K for the plasma behind the Draco nebula. Therefore we take the  $\frac{1}{4}$  keV band cross section  $\sigma(N_{\text{H}})$  for  $T = 10^{6.3}$  K as described in Snowden et al. (1994a). Deviations of the true band-averaged cross section from this model may arise if a larger amount of absorbing gas is in molecular form. Denne (1970) has found an individual  $\frac{1}{4}$  keV absorption

cross section of one hydrogen atom in an  $\text{H}_2$  molecule which is about 1.3 times larger than that of a single hydrogen atom (Henke et al. 1982). However, the effect on the total absorption cross section is small: having half the hydrogen atoms in molecular form increases the net interstellar cross section by less than 5% at 0.1 keV (Cruddace et al. 1974).

In addition, helium associated with the diffuse H II layer (Reynolds 1993) will possibly also contribute to the absorption of the distant soft X-ray source. Snowden et al. (1994b) discuss the distribution and absorption cross section of such a component for the region of the Lockman Hole (Lockman et al. 1986) and derive a value for an equivalent absorbing H I column density of  $3.4 \cdot 10^{19} \text{ cm}^{-2}$ .

#### 3.2. The method to derive $N(\text{H})$ using H I data

As discussed in Sect. 4, we regard the model parameters, i.e.  $C_{\text{Fg}}$  and  $C_{\text{Bg}}$ , to be constant over the entire region of this analysis and select all positions where only the H I column density of the diffuse galactic layer contributes to the X-ray absorption. The area of the Draco nebula is excluded in this first step. The subsequent fit of the two-component model (Eqs. (4) and (5)) to the observed soft X-ray distribution gives a first estimate of the intensity of the X-ray emission in front ( $C_{\text{Fg}}$ ) of the Draco nebula and behind ( $C_{\text{Bg}}$ ).

Next, we take these parameters to predict an observed count rate,  $C_{\text{exp}}$ , at each position of the whole field, assuming the absorbing medium is determined by the total H I column density including the Draco nebula (see Fig. 2). At positions where significant amounts of X-ray absorbing material are not in the form of H I, the shadow in the count rates will be deeper, i.e. the observed count rate,  $C_{\text{obs}}$ , will be lower than  $C_{\text{exp}}$ . The residuals,  $C_{\text{exp}} - C_{\text{obs}}$ , indicate the presence of “missing” hydrogen, i.e. hydrogen which may be in molecular form,  $\text{H}_2$ . We interpret this excess absorbing gas as molecular hydrogen if it is coincident with the Draco nebula.

However, local variations in the soft X-ray background could also produce such residuals. In order to search for such variations and to check whether they are responsible for the derived residuals, we test the two-component model in several smaller regions of the Draco nebula (see Fig. 6). The results are presented in Sects. 4.1 and 4.2.

##### 3.2.1. The fit procedure

We fit the two-component model to the observed ( $C_{\text{obs}}, N(\text{H I})$ ) (Sect. 4) and ( $C_{\text{obs}}, I_{100}$ ) (Sect. 5) data pairs by using the method of non-linear least-square fits. The count rates are weighted by their individual  $1\sigma$  errors. The uncertainties of the derived parameters are calculated using the covariance matrix method which gives similar results as the method described in Lampton et al. (1976). To compare the significance of the numerical fits we give the reduced  $\chi^2$  ( $\chi_{\text{red}}^2 = \chi_{\text{obs}}^2 / \chi_{0.05}^2$ ) values for a level of significance of 0.05. However, the  $\chi^2$  test is of minor importance to prove the physical significance of the fit results. It requires a sufficient coverage of both fit variables,  $C_{\text{obs}}$  and

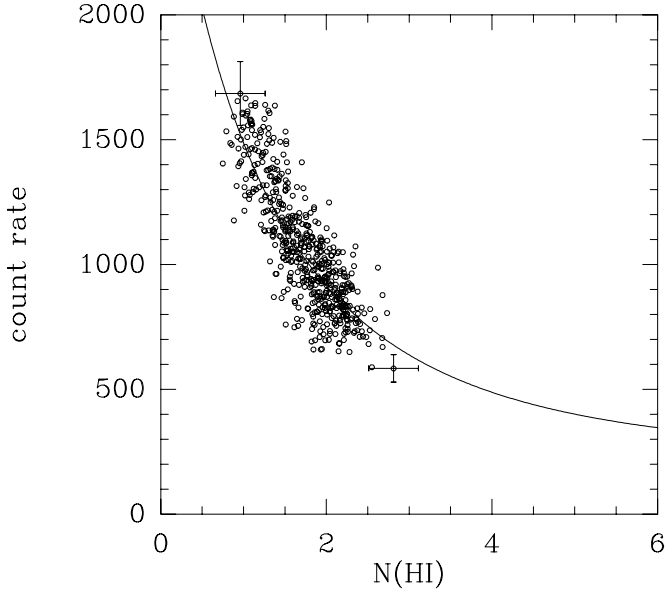


**Fig. 4.** Scatter plot of the  $(N(\text{H I}), C_{\text{obs}})$  data pairs for the diffuse galactic H I layer showing their anticorrelation. The soft X-ray count rates are given in  $10^{-6}$  counts  $\text{s}^{-1}$  arcmin $^{-2}$ ; the column densities are given in  $10^{20}$  cm $^{-2}$ . The plotted curve is representing the best-fit solution for the two-component model (Eqs. (4) and (5)). We get  $C_{\text{Fg}} = (230 \pm 30) 10^{-6}$  counts  $\text{s}^{-1}$  arcmin $^{-2}$  and  $C_{\text{Bg}} = (2730 \pm 100) 10^{-6}$  counts  $\text{s}^{-1}$  arcmin $^{-2}$ .

$N(\text{H I})$  (respectively  $I_{100}$ ), with data pairs in the  $(N(\text{H I}) [I_{100}], C_{\text{obs}})$ -diagram. This is tested by the normalized variances,  $\sigma_{C,n}^2$  and  $\sigma_{\tau,n}^2$ , the variances of the mean observed count rates and the variances of the mean optical depth  $\tau$  respectively, normalized to the scatter expected on the basis of observational errors ( $\Delta N(\text{H I}) = 2 \cdot 10^{19}$  cm $^{-2}$ ,  $\Delta I_{100} = 0.2$  MJy sr $^{-1}$ ). To be consistent with a similar analysis of Herbstmeier et al. (1995) our two free parameter fit is considered significant only if both normalized variances are  $> 2$ .

#### 4. Modelling the shadows by H I column densities

##### 4.1. Shadowing by the diffuse galactic H I layer

In this section we only consider data from regions where the X-ray absorbing medium is determined by the diffuse galactic H I, specifically, where the H I column density of the Draco nebula is lower than  $4 \cdot 10^{19}$  cm $^{-2}$ . Regions where neutral clouds exist in the LHB as well as regions where we find HVCs are excluded (see last section). The latitude interval of the dataset covers the range from  $b = 35^\circ$  to  $b = 40.5^\circ$  and the longitude interval from  $l = 88.5^\circ$  to  $l = 95^\circ$ . The scatter plot of the data from the selected regions is shown in Fig. 4, together with the best-fit solution for the two-component model (Eqs. (4) and (5)). The fit results are listed in Table 1 under the field name “DG H I”. The coverage of the data axes is sufficient to get significant results ( $\sigma_{C,n}^2 = 6.3$ ,  $\sigma_{\tau,n}^2 = 2.8$ ).

We derive a mean foreground count rate of  $(230 \pm 30) 10^{-6}$  counts  $\text{s}^{-1}$  arcmin $^{-2}$ . This value is about a factor 2 smaller than the  $\frac{1}{4}$  keV LHB count rate derived by an analysis of a PSPC

pointed observation towards the Draco nebula (Kerp 1994) and about a factor 3 smaller than the foreground count rate derived by a similar analysis of ROSAT survey data in the direction towards the HVC complex M (Herbstmeier et al. 1995). The larger foreground count rate found in the pointed observation is possibly due to problems with the contamination due to long-term enhancements (see Sect. 2.1). If we identify the local component as emission from the LHB, the larger foreground count rate found in the direction towards complex M suggests an about 1.5 times larger extend of the LHB in that direction than towards the Draco nebula. Note that Herbstmeier et al. (1995) adopt a background plasma temperature of  $10^{6.0}$  K which implies a larger absorption cross section. Assuming this temperature our foreground count rate rises to  $C_{\text{Fg}} = 400 \cdot 10^{-6}$  counts  $\text{s}^{-1}$  arcmin $^{-2}$ .

The mean background count rate is  $(2730 \pm 100) 10^{-6}$  counts  $\text{s}^{-1}$  arcmin $^{-2}$ . Kerp (1994) finds that the contribution of extragalactic sources to the distant  $\frac{1}{4}$  keV emission is low in the Draco region. If we identify this component as emission from the galactic halo we can conclude that in the  $\frac{1}{4}$  keV band the galactic halo in the region of the Draco nebula is about 12 times brighter than the LHB. This is larger than the value of 7.6 found by Snowden et al. (1991) for a smaller part of the Draco nebula around region E (see Fig. 6) by comparing preliminary ROSAT  $\frac{1}{4}$  keV band data with H I column densities. Again, this difference can be explained by the different cross sections used: for  $T = 10^6$  K we get  $C_{\text{Bg}} = 2900 \cdot 10^{-6}$  counts  $\text{s}^{-1}$  arcmin $^{-2}$  and thus a background to foreground ratio of 7.25, in good agreement with the results of Snowden et al. (1991). A background to foreground ratio of  $< 2.5$  is found by Burrows & Mendenhall (1991). This rather small value is derived from a comparison of ROSAT pointed observation with IRAS  $100 \mu\text{m}$  emission around region A (see again Fig. 6). These authors, however, neglect the absorption by the diffuse galactic layer. Therefore their results can not be compared with the other values.

We have calculated the X-ray emission measures,  $EM_{\text{LHB}}$  and  $EM_{\text{dist}}$ , by assuming a Raymond & Smith (1977) spectrum with temperatures  $T_{\text{LHB}} = 10^{5.85}$  K and  $T_{\text{dist}} = 10^{6.3}$  K. The derived foreground count rate,  $C_{\text{Fg}} = 230 \cdot 10^{-6}$  counts  $\text{s}^{-1}$  arcmin $^{-2}$ , corresponds to  $EM_{\text{LHB}} = 0.0011$  cm $^{-6}$  pc.  $C_{\text{Bg}} = 2730 \cdot 10^{-6}$  counts  $\text{s}^{-1}$  arcmin $^{-2}$  corresponds to  $EM_{\text{dist}} = 0.0055$  cm $^{-6}$  pc. The ratio  $EM_{\text{LHB}}/EM_{\text{dist}} = 0.2$  is in agreement with the value derived by Kerp (1994) whereas our absolute values are lower by about a factor of 2.

Furthermore, if we include the diffuse H II layer into our analysis by taking the equivalent H I column density of  $3.4 \cdot 10^{19}$  cm $^{-2}$  (see Sect. 3.1) and assuming that this layer is located in front of the background X-ray emission, the derived background count rate would increase by  $590 \cdot 10^{-6}$  counts  $\text{s}^{-1}$  arcmin $^{-2}$ , i.e.  $EM_{\text{dist}}$  would be about 20% larger than the value derived above. While this correction is uncertain, placement of the X-ray emission on the far side of the H II layer provides a reasonable upper limit to the halo emission.

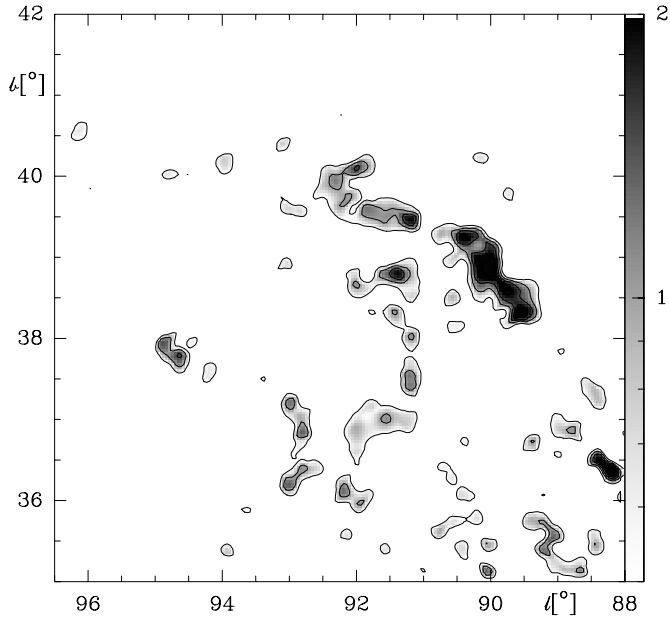


**Fig. 5.** The map of the excess absorbing hydrogen column density in the region of the Draco nebula,  $N_{\text{exc}}$ , derived from the two-component model fit for the diffuse galactic H I. The contour levels are plotted from  $0.5$  to  $2.5 \cdot 10^{20}$  atoms  $\text{cm}^{-2}$  in steps of  $0.5 \cdot 10^{20}$  atoms  $\text{cm}^{-2}$ .

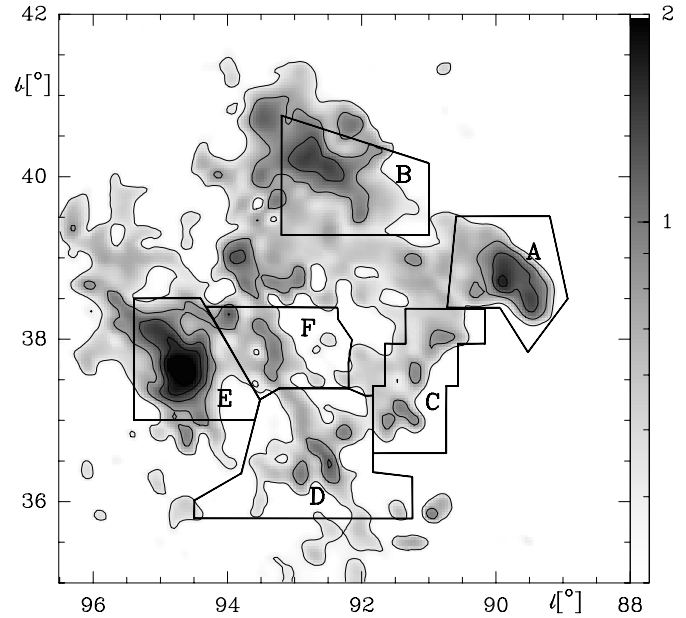


**Fig. 6.** Regions of the Draco nebula for which separate analyses are performed as an overlay on the H I column density distribution of the Draco nebula. The column densities are derived from a gaussian decomposition of the 21-cm spectra as described in Sect. 2.2. Contours are plotted beginning at  $0.4 \cdot 10^{20}$  in steps of  $0.4 \cdot 10^{20}$  atoms  $\text{cm}^{-2}$ .

#### 4.2. Shadowing by the Draco nebula

We adopt the derived foreground and background intensities for the whole Draco region and calculate the residuals,  $C_{\text{exp}} - C_{\text{obs}}$ , as described in Sect. 3. The distribution of the excess column density,  $N_{\text{exc}}$ , which must be added to the observed H I column densities to reduce the expected count rates to those observed is shown in Fig. 5. We show only column densities above  $4 \cdot 10^{19} \text{ cm}^{-2}$  which are clearly above the variations introduced by the uncertainties of the count rates or the column densities. Values up to  $3 \cdot 10^{20} \text{ cm}^{-2}$  are found in field A (see Fig. 6), about a factor of 2 more than the observed H I column density of the Draco nebula at that position. Note that the resulting total hydrogen column density still allows about 7% of the background photons to penetrate the nebula even at the position of maximum column density which is more than a factor of two larger than the uncertainty of the observed count rate.

The features displayed by Fig. 5 (except those at positions below  $l = 90^\circ$  and  $b = 37.5^\circ$ ; these positions have been excluded from the fit) show a good positional coincidence to the bright H I filaments of the Draco nebula (Fig. 6). An even better correlation shows up between these features and the dust producing the IRAS  $100 \mu\text{m}$  intensity distribution (Fig. 3), especially in region A. This is a good hint that the missing absorbing material is molecular gas:  $N_{\text{exc}} = 2 N(\text{H}_2)$ . The features below  $l = 90^\circ$  and  $b = 37.5^\circ$  are due to LVC 88+36-2 where the two-component model is not valid (see Sect. 3.1).

##### 4.2.1. Variations of the SXRb across the Draco nebula

Not only the molecular hydrogen content but also the fore- and background X-ray emission may vary across the  $N_{\text{exc}}$  image. Therefore, we derive the parameters of the two-component model in selected regions of the Draco nebula. These regions are defined by Fig. 6 and displayed as overlays to the H I column density (see Sect. 2.2). The choice of the fields follows HHM. We have selected all regions where we expect molecular hydrogen (regions A through E), but exclude the region around  $(l, b) = (91.5^\circ, 38.5^\circ)$  where larger amounts of high velocity gas are found. For the same reason, we exclude those points at the northern boundaries of region A and B from the fit, which were also left out of the fit using the diffuse H I. In addition, we take one field (region F) where we see filamentary structure in  $I_{100}$  and H I but no significant amounts of excess hydrogen (Fig. 5).

Fig. 7 shows the scatter plots of the  $(N(\text{H I}), C_{\text{obs}})$  data pairs for the selected fields, the curves represent the solutions for the two-component models listed in Table 1. Preliminary fits have been performed using only points with  $C_{\text{obs}} > 700 \cdot 10^{-6} \text{ counts s}^{-1} \text{ arcmin}^{-2}$ . This has been done so that the results will not or only marginally be affected by the deep shadows produced by the molecular gas. A two-component fit enclosing all data pairs would lead to a negative foreground count rate. However, this restriction does reduce the statistical significance of the fits so that the criterion  $\sigma_{\tau, n}^2 > 2$  (see Sect. 3.2) is not fulfilled. Therefore we fix the foreground count rate to the value  $C_{\text{Fg}} = (230 \pm 30) \cdot 10^{-6} \text{ counts s}^{-1} \text{ arcmin}^{-2}$ , the value derived for the diffuse H I layer. This assumption seems reasonable because it is unlikely that the foreground count rate does vary by more

**Table 1.** Fit results

Region	$C_{\text{Fg}}$ ( $10^{-6}$ counts $\text{s}^{-1}$ arcmin $^{-2}$ )	$C_{\text{Bg}}$ ( $10^{-6}$ counts $\text{s}^{-1}$ arcmin $^{-2}$ )	points	$\chi^2_{\text{red}}$
DG H I	$230 \pm 30$	$2730 \pm 100$	559	1.20
A	230(fixed)	$2520 \pm 120$	29	0.40
B	230(fixed)	$2460 \pm 140$	44	1.30
C	230(fixed)	$2630 \pm 130$	43	0.60
D	230(fixed)	$2750 \pm 140$	77	0.99
E	230(fixed)	$2950 \pm 160$	38	1.03
F	230(fixed)	$2910 \pm 140$	51	1.44

than 15% on scales of a few degrees if there are no individual dense clouds along the sightlines in the LHB.

The fit results are listed in Table 1. The columns give the field name (column 1), foreground count rate,  $C_{\text{Fg}}$ , in units of  $10^{-6}$  counts  $\text{s}^{-1}$  arcmin $^{-2}$  (column 2), background count rate,  $C_{\text{Bg}}$ , in units of  $10^{-6}$  counts  $\text{s}^{-1}$  arcmin $^{-2}$  (column 3), number of data points used (column 4), and the  $\chi^2_{\text{red}}$  (column 5). Here the H I errors have been transformed into an additional count rate error by estimating the difference between  $C_{\text{exp}}(N(\text{H}))$  and  $C_{\text{exp}}(N(\text{H}) \pm \Delta N(\text{H}))$  for a given background count rate of  $2700 \cdot 10^{-6}$  counts  $\text{s}^{-1}$  arcmin $^{-2}$ .

The values of  $\chi^2$  show that the two-component model gives a good solution for the SXRb. The somewhat larger  $\chi^2$  value of the DG fit in comparison to most of the other fits are possibly due to slight variations in the background intensity (see above). It is also possible that unresolved X-ray sources producing small-scale variations in the SXRb, or larger true errors in the H I column densities than the adopted measurement error of  $2 \cdot 10^{19}$  cm $^{-2}$  (regions B and F), can be the reason for the enhanced  $\chi^2$  values. The derived background count rates show that the intensity of the halo emission component does not vary strongly across the region of the Draco nebula. We find only a weak intensity gradient in the distant component from the north-west (regions A and B) to the south-east (regions E and F). However, none of the derived values differs by more than 10% from the average intensity of the whole field. This fact also justifies our assumption of a constant foreground intensity: Due to the strong correlation between  $C_{\text{Fg}}$  and  $C_{\text{Bg}}$  in the fit procedure a reduced foreground intensity would result in a larger background intensity and vice versa.

#### 4.2.2. A non-constant plasma temperature

In our analysis we have adopted a constant temperature of  $10^{6.3}$  K for the plasma behind the Draco nebula, derived by an analysis of the whole X-ray spectrum (Kerp 1994). However, it can not be ruled out that this plasma has a temperature gradient which depends on distance to the galactic plane if we bear in mind that the temperature of the local component ( $10^{5.85}$  K, Kerp 1994) is significantly lower. Such a gradient has been predicted by the model of Hirth et al. (1991). In this case the distribution of the  $\frac{1}{4}$  keV photons would be shifted to smaller energies because the

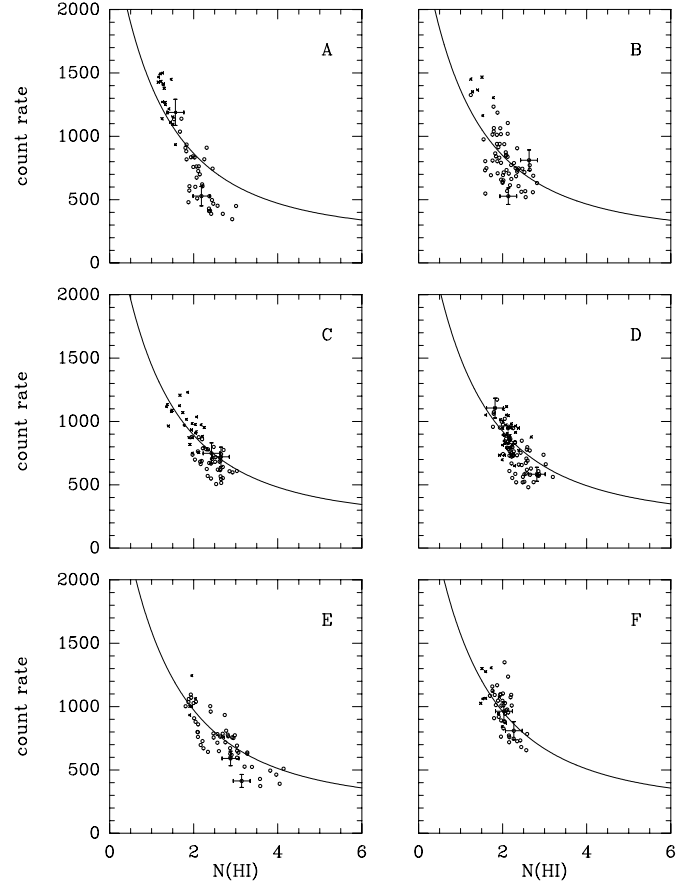


**Fig. 7a-f.** Scatter plots of the  $(N(\text{H I}), C_{\text{obs}})$  data pairs for the regions of the Draco nebula. The soft X-ray count rates are given in  $10^{-6}$  counts  $\text{s}^{-1}$  arcmin $^{-2}$ . The column densities are given in  $10^{20}$  cm $^{-2}$ . The plotted curves represent preliminary fits to the two-component model (only data pairs with  $C_{\text{obs}} > 700 \cdot 10^{-6}$  counts  $\text{s}^{-1}$  arcmin $^{-2}$  are used for the fits) for a fixed foreground count rate  $C_{\text{Fg}} = 230 \cdot 10^{-6}$  counts  $\text{s}^{-1}$  arcmin $^{-2}$ . Crosses represent points with  $N(\text{H I, DN}) < 3 \cdot 10^{19}$  cm $^{-2}$  ("OFF"), circles represent points with  $N(\text{H I, DN}) > 3 \cdot 10^{19}$  cm $^{-2}$  ("ON").

amount of emitted photons in this energy range has a maximum at a temperature between  $10^{6.0}$  K and  $10^{6.1}$  K (Raymond & Smith 1977).

The direct consequence of a lower temperature for our model is an increase of the band-averaged absorption cross section. Numerically, the fit results for the foreground count rate,  $C_{\text{Fg}}$ , is more sensitive to variations of the absorption cross section than the distant count rate,  $C_{\text{Bg}}$ . For increasing cross section  $\sigma$  and increasing  $C_{\text{Bg}}$ , which both lead to a stronger negative gradient, a good fit can only be achieved by a simple shift of the curve towards larger count rates, i.e. by an increase of  $C_{\text{Fg}}$ . In addition, there is only a small number of data points at low count rates (large column densities) which could give more stringent limits to  $C_{\text{Fg}}$ . However, the increasing cross section (together with the corresponding larger  $C_{\text{Fg}}$ ) does not strongly affect the resulting mean excess absorbing column densities. We have verified that for  $T = 10^{6.0}$  K these values do not differ by more than 20% from those for a background plasma with  $T = 10^{6.3}$  K. However,

we have to note that for  $T = 10^{6.0}$  K the resulting values for  $C_{\text{Fg}}$  are larger than the lowest observed count rates. Since the two should be identical, this is an unphysical result. Hence only a lower limit for the maximum absorbing column density can be given.

#### 4.2.3. The excess column density

The diagrams in Fig. 7, in particular that for region A, show that the data pairs with low count rates fall far below the fit curve. This is due to the deep depression in the count rates which can not be explained by H I alone. Also in the other diagrams (mainly for regions B, C and D) a large part of the data points lies below the model curve. However, the scatter in these diagrams is markedly larger than in the data points of region A.

The missing column density at each position of our maps can be read directly from Fig. 7 by estimating the horizontal distance of the data points to the model curve. A point which lies below the model curve shows excess column density which means that there is more absorbing hydrogen than indicated by H I. A point significantly above the curve indicates an enhanced background count rate. Of course, points below the curve can also be due to a reduced or enhanced background count rate.

Although we excluded points with low X-ray count rates from the fit, we can not rule out that the fit is still biased by data which are affected by molecular hydrogen. In order to test this we checked the regions where the X-ray absorbing gas is completely determined by H I. If molecular hydrogen is still present we would expect an excess of absorbing gas at the "ON"-positions ( $N(\text{H I}, \text{DN}) > 3 \cdot 10^{19} \text{ cm}^{-2}$ ) which have been included in the fit, i.e. a significant deviation of the corresponding data points below the fitted two-component model. However, this is not the case: for all regions the average excess column density at these points is zero within its limits.

In Table 2 we list the average and the maximum excess hydrogen column densities for the different subregions. In order to make sure that the excess hydrogen is indicative of molecular gas belonging to the Draco nebula, we distinguish between points where  $N(\text{H I}, \text{DN}) > 3 \cdot 10^{19} \text{ cm}^{-2}$  (ON) and points where only H I of the diffuse galactic layer (OFF) is seen. We do not find any excess of X-ray absorbing gas outside the area of the Draco nebula. In the corresponding parts of regions C through to F the average of the excess column density is zero within the error limits.

We find negative values for the excess in region A and in particular in region B. This indicates excess X-ray emission from the background, since these values are mainly found at the galactic northern boundary of the Draco nebula, i.e. at positions which have been excluded from the fit. For this part of region B we derive a background count rate of  $C_{\text{Bg}} = 3200 \cdot 10^{-6} \text{ counts s}^{-1} \text{ arcmin}^{-2}$  which is about 17% larger than the value found for the DG-fit. The enhancement is obviously associated with the HVCs north of the area (Kerp et al. 1994).

In all regions "ON" the Draco nebula – except region F – we detect excess absorbing gas. At least 80% of the excess

hydrogen is found at those positions which have been excluded from the fit. The largest fraction of excess hydrogen is found in the south-west boundary of the Draco nebula. In region A only about 50% of the optical depth comes from H I gas, in regions C and D about 65%. This means that in these parts of the nebula about 35 to 50% of the neutral hydrogen are bound in molecules, in the densest parts even 70%. In the other regions the average molecular abundance is not larger than 20% whereas the maximum values are around 50%.

#### 4.3. The correlation between $N_{\text{H}}$ and $I_{100}$

To give further evidence that the excess X-ray absorbing gas is molecular hydrogen in the Draco nebula we analyse the correlation between the derived total hydrogen column density and the FIR-intensity at  $100 \mu\text{m}$ . The FIR-intensity,  $I_{100}$ , can be regarded as a linear measure of the total hydrogen column density in diffuse clouds at high galactic latitudes, if the dust temperature is isothermal and the gas-to-dust ratio constant (see Sect 2.3). Independently,  $N_{\text{exc}}$  has been determined in such a way that the column density of hydrogen nuclei calculated from  $N_{\text{H, DN}} = N(\text{H I}) + N_{\text{exc}}$  is a linear measure of the total X-ray absorbing material. Assuming that  $N_{\text{exc}} = 2 \cdot N_{\text{H}_2}$ , i.e. the excess X-ray absorbing material is molecular hydrogen gas belonging to the Draco nebula we expect a linear relation between  $I_{100}$  and  $N_{\text{H, DN}}$ . In Fig. 8 (right) we show the corresponding diagrams. For all fields a linear correlation is found within the limits of the observational and methodical errors.

In Table 3 the results of the best linear fits are given, represented by the solid lines in Fig. 8 (right). For these fits, we have only considered those points where the column density and the FIR-emission are significant. The slopes of these lines correspond to the FIR-emissivity per hydrogen nucleon of the Draco nebula,  $a_{100, \text{DN}}$  (column 2). The offset  $I_{\text{off}}$  (column 3) is zero within the error limits. This means that the contribution from material in front or behind the Draco nebula has been subtracted adequately (see Sect. 2.3). Due to the large uncertainties of the column density (about  $4 \cdot 10^{19} \text{ cm}^{-2}$ ) the correlation coefficients (column 4) are somewhat low, in particular for region C.

The FIR-emissivity of  $(1.02 \pm 0.24) \cdot 10^{-20} \text{ MJy sr}^{-1} \text{ cm}^2$  derived for the entire nebula (field name DRN) is only slightly larger than the value found for the diffuse galactic H I layer and is consistent with the average value of  $(1.11 \pm 0.05) \cdot 10^{-20} \text{ MJy sr}^{-1} \text{ cm}^2$  found for the Draco nebula from a comparison between  $I_{100}$ ,  $N(\text{H I})$  and  $W(^{12}\text{CO})$  (see HHM).

The deviations of the FIR-emissivity in the different subregions from one-another, and from that for the entire nebula, are not significant. This is different from what one finds from a correlation of the FIR-intensity with just the H I column density (see Column 5 of Table 3). For a better comparison the offsets have been set to zero. Here one finds large deviations between the different regions (see Fig. 8, left column). We see that these deviations correlate with the amount of excess hydrogen (see Table 2). This is due to the presence of molecular hydrogen which affects the quality of the correlations between  $I_{100}$  and  $N(\text{H I})$ . In particular, the large value for region A

**Table 2.** Average and maximum H I and excess absorbing column densities

Region	pts. ON	$\overline{N(\text{H I}, \text{DN})}$ ( $10^{20} \text{ cm}^{-2}$ )	$\max(N(\text{H I}, \text{DN}))$ ( $10^{20} \text{ cm}^{-2}$ )	$\overline{N_{\text{exc}}, \text{ON}}$ ( $10^{20} \text{ cm}^{-2}$ )	$\max(N_{\text{exc}}, \text{ON})$ ( $10^{20} \text{ cm}^{-2}$ )	pts. OFF	$\overline{N_{\text{exc}}, \text{OFF}}$ ( $10^{20} \text{ cm}^{-2}$ )
A	37	0.85	1.6	$0.88 \pm 0.06$	$2.9 \pm 0.4$	20	$-0.18 \pm 0.08$
B	64	0.78	1.4	$0.17 \pm 0.05$	$1.7 \pm 0.5$	6	$-0.43 \pm 0.16$
C	40	0.59	1.0	$0.32 \pm 0.06$	$1.0 \pm 0.4$	26	$-0.05 \pm 0.07$
D	65	0.56	1.2	$0.29 \pm 0.05$	$1.5 \pm 0.5$	40	$0.00 \pm 0.06$
E	54	1.05	2.4	$0.22 \pm 0.06$	$2.1 \pm 0.5$	6	$-0.11 \pm 0.16$
F	41	0.61	1.2	$0.01 \pm 0.06$	$0.6 \pm 0.4$	12	$0.04 \pm 0.11$

**Table 3.** FIR-emissivities

Region	$a_{100, \text{DN}(\text{H})}$ ( $10^{-20} \text{ MJy sr}^{-1} \text{ cm}^2$ )	$I_{\text{off}}$ ( $\text{MJy sr}^{-1}$ )	$r$	$a_{100, \text{DN}(\text{H I})}$ ( $10^{-20} \text{ MJy sr}^{-1} \text{ cm}^2$ )	$a_{100}(\text{HHM})$ ( $10^{-20} \text{ MJy sr}^{-1} \text{ cm}^2$ )
DRN	$1.02 \pm 0.24$	$-0.03 \pm 0.23$	0.79	$1.69 \pm 0.31$	$1.11 \pm 0.05$
A	$1.07 \pm 0.21$	$0.18 \pm 0.38$	0.82	$2.57 \pm 0.10$	$1.8 \pm 0.4$
B	$0.92 \pm 0.37$	$0.24 \pm 0.40$	0.64	$1.47 \pm 0.09$	$1.66 \pm 0.04$
C	$1.07 \pm 0.46$	$0.24 \pm 0.45$	0.50	$2.09 \pm 0.05$	$1.22 \pm 0.04$
D	$0.93 \pm 0.15$	$-0.13 \pm 0.08$	0.67	$1.61 \pm 0.08$	$1.62 \pm 0.09$
E	$0.92 \pm 0.17$	$-0.24 \pm 0.24$	0.83	$1.06 \pm 0.09$	$1.28 \pm 0.05$
F	$0.88 \pm 0.20$	$-0.12 \pm 0.16$	0.80	$0.92 \pm 0.10$	$1.0 \pm 0.1$

( $2.57 \cdot 10^{-20} \text{ MJy sr}^{-1} \text{ cm}^2$ ) shows that here the majority of the X-ray absorbing material is in the form of molecular hydrogen.

However, we note that our  $a_{100}(\text{H})$  values are lower than the results of HHM for the dust mixed with H I gas only, in particular in regions A, B and D, where molecular hydrogen is found. For comparison we present their FIR-emissivities in the last column of Table 3 (the value for region C is the average from their regions D1, D2 and D3). For region F, where no molecular hydrogen is found, the values of both analyses agree reasonably well. The  $a_{100}$  value of HHM for region E is probably an overestimate since some of the observed  $W(^{12}\text{CO})$  values have not been used in the fit. Including these data, Herbstmeier (1990) derives  $a_{100} = (0.92 \pm 0.08) \cdot 10^{-20} \text{ MJy sr}^{-1} \text{ cm}^2$  in good agreement with our result. The differences between the HHM values and ours for the other fields can be explained by the more detailed approach of HHM. In contrast to our study the authors attempted to disentangle the contribution of the dust emission in the molecular cores and their associated H I haloes.

#### 4.4. The $x_{W\text{CO}}$ factor

The CO molecule is used as a tracer of molecular hydrogen. However, the  $^{12}\text{CO}$  line intensity is not suitable to calculate  $N(\text{H}_2)$  directly. The conversion factor,  $x_{W\text{CO}} \equiv N(\text{H}_2)/W(^{12}\text{CO})$ , depends on physical properties of the cloud like its kinetic temperature (e.g. Kutner & Leung 1985; Maloney & Black 1988), the radiation field, and the CO abundance. Since we have estimated the molecular hydrogen column densities by

a method which is independent of CO emission, we now have a direct means to calculate the  $x_{W\text{CO}}$  factor.

CO has been detected in all regions where we find evidence for  $\text{H}_2$ . Consistent with the non-detection of  $\text{H}_2$  by X-ray shadowing, CO has not been detected in region F. In region B, CO has been searched for in only a very few positions so that we can not derive a useful conversion factor. CO has also been detected in the centre region of the Draco nebula. But here the anticorrelation between  $N(\text{H I})$  and the X-ray intensity is too weak for a reliable determination of the total absorbing hydrogen.

In general, the correlation between  $W(^{12}\text{CO})$  and  $N(\text{H}_2)$  ( $\equiv 0.5 N_{\text{exc}}$ ) in the Draco nebula is weak (see Fig. 9) for which we do not have a simple explanation. Herbstmeier (1990) has carefully checked the positional accuracy of the CO spectra. We can also rule out that the weak correlation is due to a non perfect matching of the different pixel sizes. HHM, however, have also found hints for only weak correlation between  $W(^{12}\text{CO})$  and  $N(\text{H}_2)$  in different parts of the Draco nebula.

As can be seen from Fig. 9 linear fits are not useful to estimate the  $x_{W\text{CO}}$  ratio. Therefore we give the average conversion factor,  $\overline{x_{W\text{CO}}} = \overline{N_{\text{exc}}(\text{H})}/(2 \overline{W(^{12}\text{CO})})$ , for the regions defined in Fig. 6 (see Table 4). We take all positions where  $N(\text{H I}, \text{DN}) > 3 \cdot 10^{19} \text{ cm}^{-2}$ , i.e. the same area is used for calculating the mean excess column density and the mean CO line integral. For region B we only consider the positions where data for CO and  $\text{H}_2$  exist.

All values for the selected regions - except for region C - are in the range  $0.34 < x_{W\text{CO}} < 0.52 \cdot 10^{20} \text{ cm}^{-2} (\text{K km s}^{-1})^{-1}$ , a range which is typical for clouds in the galactic cirrus (see Ta-

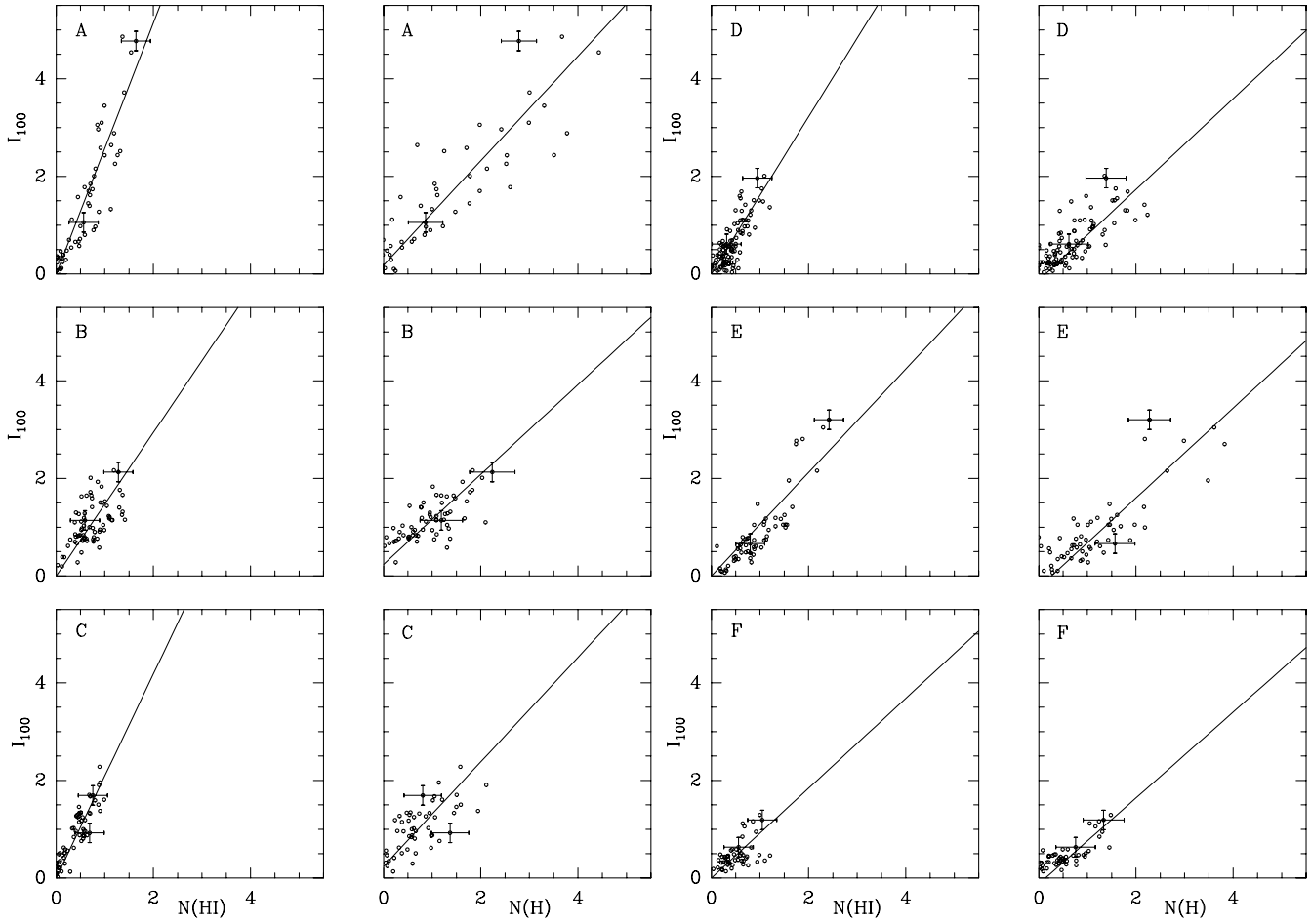


**Fig. 8.** left: The scatter diagrams of the  $(N(\text{H I}), I_{100})$  data pairs for the regions of the Draco nebula defined in Fig. 6. The column densities are in units of  $10^{20}$  atoms  $\text{cm}^{-2}$ , the FIR-intensities in units of  $\text{MJy sr}^{-1}$ . Note the strong deviation of the slopes in the different regions. right: The scatter diagrams of the  $(N(\text{H}), I_{100})$  pairs ( $N(\text{H}) \equiv N(\text{H I}) + 2 N(\text{H}_2)$ ). The lines represent the best linear fits performed for the points where  $N(\text{H})$  and  $I_{100}$  are significant. The slope of these lines, the FIR-emissivity per hydrogen nucleon,  $a_{100}(\text{H})$ , shows only slight variations between the different subregions.

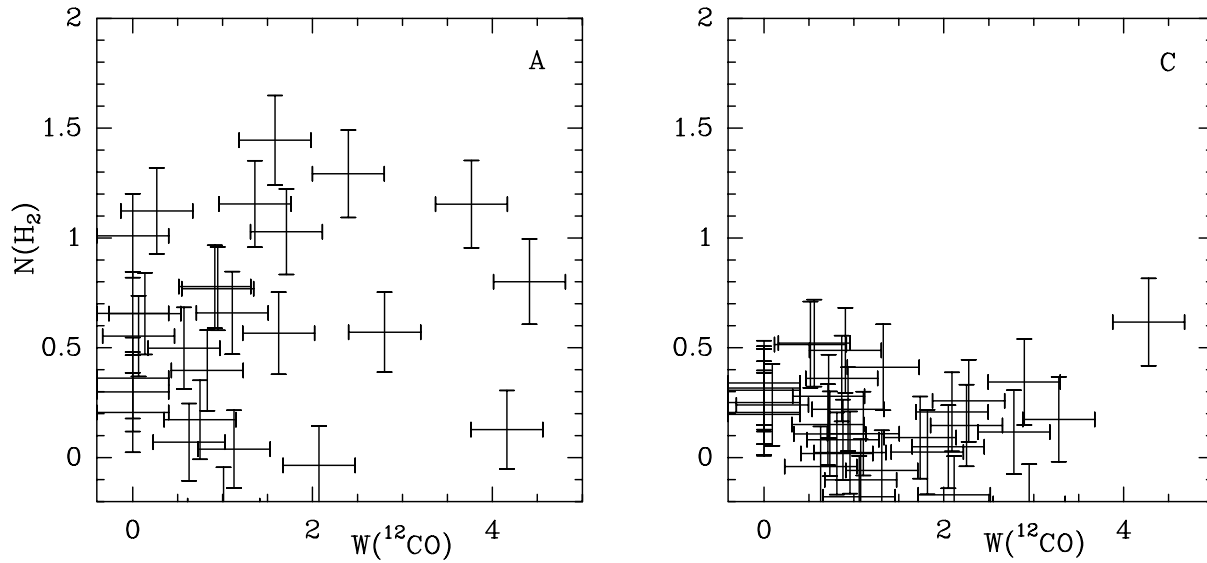


**Fig. 9.** The molecular hydrogen column density,  $N(\text{H}_2)$ , in units of  $10^{20}$  atoms  $\text{cm}^{-2}$  versus the  $^{12}\text{CO}$  line integral,  $W(^{12}\text{CO})$ , in units of  $\text{K s}^{-1}$  for region A (left) and region C (right).

ble 4). The value of  $0.17 \cdot 10^{20} \text{ cm}^{-2} (\text{K km s}^{-1})^{-1}$  found in region C is more than a factor of 2 smaller than that for the other selected regions (see Fig. 9). While this trend has also been found by HHM their  $x_{WCO}$  factors ( $0.02 < x_{WCO} < 0.26 \cdot 10^{20} \text{ cm}^{-2} (\text{K km s}^{-1})^{-1}$ ) are even lower than ours.

These low  $x_{WCO}$  ratios have been used as evidence for a collisional interaction between HVCs (or high- $z$  galactic gas) and the Draco nebula (see HHM). These authors argue that such an interaction takes place at the edge towards low galactic longitudes and latitudes where the CO abundance is altered in a low velocity shock.

The  $x_{WCO}$  ratio of the total Draco nebula,  $x_{WCO}(\text{DN}) = 0.24 \cdot 10^{20} \text{ cm}^{-2} (\text{K km s}^{-1})^{-1}$ , calculated using the fit results for the diffuse background, is smaller than the ratio in most of the selected regions. This is due to the fact that in several regions of the Draco nebula the mean observed count rates are larger than the mean expected ones which formally is leading to negative excess column densities and therefore to a too low mean  $\text{H}_2$  column density. Therefore it is more reliable to use only the positions where  $\text{H}_2$  and CO have been detected for the derivation of  $x_{WCO}(\text{DN})$ . Then we get  $x_{WCO}(\text{DN}) = 0.39 \cdot 10^{20} \text{ cm}^{-2} (\text{K km s}^{-1})^{-1}$  which is more consistent with the results of the selected regions.

#### 4.5. Determination of mass and extinction

The mean total hydrogen column densities in the different subregions of the Draco nebula are in the range  $0.6 \leq \overline{N(\text{H})} \leq 1.7 \cdot 10^{20} \text{ cm}^{-2}$  (see Table 2). Using the standard gas-to-dust ratio  $N(\text{H})/A_V = 1.87 \cdot 10^{21} \text{ cm}^{-2} \text{ mag}^{-1}$  of Bohlin et al. (1978), we derive very low mean values of the visual extinction  $0.03 \text{ mag} \leq \overline{A_V} \leq 0.09 \text{ mag}$ . The maximum hydrogen column density of  $4.5 \cdot 10^{20} \text{ cm}^{-2}$  (region A) corresponds to a visual extinction of  $A_V(\text{max}) \simeq 0.25 \text{ mag}$ .

The values for  $A_V$  are very low, especially for regions A and D where more complex molecules such as  $\text{H}_2\text{CO}$  and  $\text{NH}_3$  have been found (Mebold et al. 1985; Mebold et al. 1987). Additional results from star counts require a lower limit of  $\overline{A_{V,\text{min}}} = 0.2$  for region A (Rohlf 1986). Therefore we agree with the conclusion of HHM that the gas-to-dust ratio of Bohlin et al. (1978) is probably too large at least by a factor of 2 for the Draco nebula.

In Table 4 we list the  $\text{H}_2$  mass and the total masses for all subregions. Furthermore we list the solid angles  $\Omega$  over which the averages of the column densities (see Table 2) and CO line integrals are derived.  $\Omega$  is the sum of the sampled beam areas scaled by the undersampling correction factor  $4/\pi$  for an orthogonal grid. The gas masses have been calculated from the column densities and the areas  $\Omega$  assuming a distance of  $D = 500 \text{ pc}$  for the Draco nebula.

In Row 1 of Table 4 we give the total molecular mass of the Draco nebula using the mean excess column density  $\overline{N_{\text{exc}}(\text{H})} = 0.11 \cdot 10^{20} \text{ cm}^{-2}$ , derived from the solution of the radiation transport for the diffuse galactic H I. For the same reason why the  $x_{WCO}$  ratio derived for the total Draco nebula is smaller than for most of the subregions (see Sect. 4.4), this value is smaller than the total  $\text{H}_2$  mass found in the subregions.

**Table 4.**  $x_{WCO}$ , areas,  $\text{H}_2$  and total masses and visual extinctions of the regions of the Draco nebula

Re.	$\overline{x_{WCO}}$ ( $\text{cm}^{-2} (\text{K km s}^{-1})^{-1}$ )	$\Omega$ ( $10^{-4} \text{ sr}$ )	$M(\text{H}_2)$ ( $M_\odot D^2 (500 \text{ pc})^{-2}$ )	$M(\text{H})$ ( $M_\odot D^2 (500 \text{ pc})^{-2}$ )
tot	$(0.24 \pm 0.06) \cdot 10^{20}$	56.89	$97 \pm 14$	$696 \pm 18$
A	$(0.52 \pm 0.05) \cdot 10^{20}$	3.67	$51 \pm 4$	$100 \pm 5$
B	$(0.46 \pm 0.22) \cdot 10^{20}$	6.35	$17 \pm 5$	$95 \pm 6$
C	$(0.17 \pm 0.07) \cdot 10^{20}$	3.97	$20 \pm 4$	$57 \pm 5$
D	$(0.44 \pm 0.08) \cdot 10^{20}$	6.45	$30 \pm 4$	$87 \pm 5$
E	$(0.34 \pm 0.09) \cdot 10^{20}$	5.36	$19 \pm 5$	$107 \pm 6$
F	-	4.07	$0 \pm 4$	$39 \pm 5$

Therefore, in the following paragraph, we take the  $\text{H}_2$  masses of the selected regions to calculate the total mass of the Draco nebula and ignore the results given in Row 1 of Table 4.

The total molecular mass found in the subregions is  $M(\text{H}_2) = (137 \pm 11) M_\odot D^2 (500 \text{ pc})^{-2}$  which is about a factor of 3 more than found by HHM. Since these subregions cover almost all regions where CO line emission has been found, we think that the other parts of the Draco nebula contain at most about 10% of the molecular mass so that we get a total molecular mass of about  $M_{\text{DN}}(\text{H}_2) = 151 M_\odot D^2 (500 \text{ pc})^{-2}$ . From the mean H I column density of the Draco nebula,  $\overline{N(\text{H I}, \text{DN})} = 0.67 \cdot 10^{20} \text{ cm}^{-2}$ , and the corresponding solid angle,  $\Omega = 56.89 \cdot 10^{-4} \text{ sr}$ , the total H I mass of the Draco nebula is derived,  $M_{\text{DN}}(\text{H I}) = 599 M_\odot D^2 (500 \text{ pc})^{-2}$ . The total hydrogen mass of the Draco nebula is thus about  $750 M_\odot D^2 (500 \text{ pc})^{-2}$ , of which approximately 20% is molecular.

The total hydrogen masses in the subregions range from 39 to  $107 M_\odot D^2 (500 \text{ pc})^{-2}$ , and are still lower than the corresponding virial masses derived by Mebold et al. (1985) if 10% He is included. It is therefore unlikely that the Draco nebula is a site of active star formation.

## 5. Modelling the shadows by the IRAS 100 $\mu\text{m}$ intensity

In the last section we have presented the most direct way (“H I method”) to estimate the total hydrogen content of the Draco nebula. This method, however, has the problem that just those positions have to be excluded from the fit where molecular hydrogen is expected. This restriction can be avoided if we express  $N(\text{H})$  in terms of the IRAS 100  $\mu\text{m}$  intensity,  $I_{100}$ , instead of H I. After  $I_{100}$  is converted into  $N(\text{H})$  according to Eq. (3), the two-component model (Eqs. (4) and (5)) can be fitted to the  $(I_{100}, C_{\text{obs}})$  data pairs using the procedure described in Sect. 3.2.1. The FIR-emissivity of the Draco nebula,  $a_{100,\text{DN}}$ , is treated as a free fit parameter. Further advantages of this method are the better spatial resolution of the IRAS data in comparison to H I and their lower relative statistical uncertainties. Disadvantages of this method are discussed below.

### 5.1. The two-component model using IRAS instead of HI

We have selected one large field containing all striking features of the Draco nebula (field name “DRN”). The results of the two-component fit are listed in Table 5, together with the results for the different subregions defined in Fig. 6 (see below). The reduced  $\chi^2$  values,  $\chi_{\text{red}}^2$ , are given for a level of significance of 0.05 (column 6). The relative variances of the X-ray count rates (column 7) and of the optical depth (column 8, estimated for  $a_{100,\text{DN}} = 1.0 \cdot 10^{-20} \text{ MJy sr}^{-1} \text{ cm}^2$ ) fulfil the requirement given in Sect. 3.2.1, but with the restriction that here we have three fit parameters (region DRN).

The fit results are consistent with the corresponding values derived by the HI method. The mean foreground count rate,  $C_{\text{Fg}} = (230 \pm 20)10^{-6} \text{ counts s}^{-1} \text{ arcmin}^{-2}$ , is identical for both methods while the mean background count rate,  $C_{\text{Bg}} = (2610 \pm 140)10^{-6} \text{ counts s}^{-1} \text{ arcmin}^{-2}$ , and the FIR-emissivity  $a_{100,\text{DN}} = (0.95 \pm 0.05) \text{ MJy sr}^{-1} \text{ cm}^2$ , found here are only slightly lower. This directly shows that the absorbing column densities are approximately equal in both methods (within about 5 to 10%). The differences are possibly due to the fact that FIR-intensity of the diffuse HI layer is modeled by a cosecant-law (see Sect. 2.3) or due to small offsets in the  $I_{100}$  intensity (see also Table 3).

For comparison we also present the fit results for the different subregions. The foreground count rate,  $C_{\text{Fg}}$ , is fixed to  $230 \cdot 10^{-6} \text{ counts s}^{-1} \text{ arcmin}^{-2}$  as with the HI fits. Here, however, the reason is a strong correlation between the fit parameters  $C_{\text{Fg}}$  and  $a_{100,\text{DN}}$  which can easily be illustrated: A variation of  $a_{100}$  results in a shift of the data points along the  $N(\text{H})$  axis. For example an increase of  $a_{100}$  shifts the data towards smaller  $N(\text{H})$  values which results in a decrease of the foreground count rate,  $C_{\text{Fg}}$ .

The background count rates are found in the range  $2570 \leq C_{\text{Bg}} \leq 2990 \cdot 10^{-6} \text{ counts s}^{-1} \text{ arcmin}^{-2}$ , the FIR-emissivities in the range  $0.78 \leq a_{100} \leq 1.11 \cdot 10^{-20} \text{ MJy sr}^{-1} \text{ cm}^2$ . With the exception of region E, the values do not differ by more than 10% from the results of the HI method. In region E, we find a background count rate which is  $340 \cdot 10^{-6} \text{ counts s}^{-1} \text{ arcmin}^{-2}$  lower than the corresponding value listed in Table 1 which implies less absorbing gas than detected by the HI method. Here HHM have found an IVC with a rather large neutral hydrogen column density (up to  $1.0 \cdot 10^{20} \text{ cm}^{-2}$ ) which is apparently not associated with dust, at least it is not seen in the  $100 \mu\text{m}$  radiation. As the centre velocity of this gas is at about  $-35 \text{ km s}^{-1}$  (see also Herbstmeier et al. 1996), it is included in what we call the diffuse HI (see Sect. 2.2). The 16% lower FIR-emissivity compared to the value of HI method (see Table 3) could be explained by the shadow in the SXR cast by the IVC which thus belongs to the new class of IVCs and HVCs that have been studied in X-ray absorption by Herbstmeier et al. (1995) and Kerp et al. (1994). In the method presented here this shadow is attributed to the Draco nebula decreasing its FIR-emissivity because the FIR-emissivity of the diffuse HI layer is fixed (Sect. 2.3).

In general the method presented in this section gives results which are consistent with those derived in Sect. 4. However, we have to note that a careful determination of the FIR-intensity distribution of the spatially isolated cloud *and* of the diffuse HI layer is required. First, their FIR-emissivity could be different. But more important, it is not - or only with severe difficulty - possible to derive the IR-intensity of the diffuse galactic layer without using the information provided by the diffuse HI gas (see Sect. 2.3). Furthermore, X-ray absorbing clouds which do not have IR-emission complicate the X-ray radiation transport, if it is formulated in terms of IR-intensities.

Independent of these disadvantages, a non-constant dust temperature or a non-constant gas-to-dust ratio imply variations in the FIR-emissivity and could lead to errors in the determination of  $N(\text{H})$ . Finally, further offsets in the IR-intensity which are possibly not associated with X-ray absorbing gas (see also HHM) can not be derived by our model fit and can therefore affect the results.

## 6. Conclusions

We have used the ROSAT  $\frac{1}{4}$  keV all-sky survey together with HI observations from Effelsberg to determine the neutral gas content of the Draco nebula, a molecular cloud which is found to produce a shadow in the soft X-ray background. The X-ray emitting plasma has been approximated by a two component model, i.e. a local unabsorbed component associated with the LHB, and a distant component including both galactic halo and extragalactic emission. This component is attenuated by the Draco nebula (distance  $> 300 \text{ pc}$ ; Lिलienthal et al. 1991) as well as by the diffuse galactic gas. To derive the foreground,  $C_{\text{Fg}}$ , and the background,  $C_{\text{Bg}}$ , X-ray intensities the two component model has been fitted to the observed count rates in regions outside the Draco nebula in order to be unaffected by molecular hydrogen.

The optical depth of the X-ray absorbing medium is calculated by using effective band averaged absorption cross sections (Snowden et al. 1994a) and the observed HI column densities. Based on the results for  $C_{\text{Fg}}$  and  $C_{\text{Bg}}$  one can calculate the optical depth also for the Draco nebula. Converting the optical depth into total hydrogen column densities and comparing these column densities to those for HI alone allows to estimate the molecular hydrogen ( $\text{H}_2$ ) content of the Draco nebula. From a comparison of the  $\text{H}_2$  column densities with observed CO line integrals we finally obtain a direct estimate of the conversion factor  $x_{\text{WCO}}$ . The optical depth has also been obtained (Sect. 5) by converting the IRAS  $100 \mu\text{m}$  intensities into total hydrogen column densities. Then the corresponding conversion factor becomes an additional free fit parameter, the FIR-emissivity per nucleon,  $a_{100}$ . This procedure leads to results for  $C_{\text{Fg}}$ ,  $C_{\text{Bg}}$  and  $a_{100}$  which are consistent with those found earlier in the present paper or in the literature.

We summarize the main results:

- The method used in the present paper (Sect. 4) is well suited to examine the X-ray emission in front and behind the absorbing cloud structures and the total absorbing hydrogen

**Table 5.** Fit results for the two-component model using  $I_{100}$  instead of H I

Region	$C_{Fg}$ ( $10^{-6}$ counts $s^{-1}$ arcmin $^{-2}$ )	$C_{Bg}$ ( $10^{-20}$ MJy sr $^{-1}$ cm $^2$ )	$a_{100, DN}$ ( $10^{-20}$ MJy sr $^{-1}$ cm $^2$ )	points	$\chi^2_{red}$	$\sigma_{C,n}^2$	$\sigma_{\tau,n}^2$
DRN	$230 \pm 20$	$2610 \pm 140$	$0.95 \pm 0.05$	849	1.45	7.7	13.2
A	230 (fixed)	$2710 \pm 170$	$1.11 \pm 0.11$	48	1.09	11.1	44.3
B	230 (fixed)	$2590 \pm 230$	$0.91 \pm 0.12$	63	0.96	4.1	8.7
C	230 (fixed)	$2570 \pm 90$	$1.01 \pm 0.07$	66	0.53	5.0	10.4
D	230 (fixed)	$2670 \pm 70$	$0.89 \pm 0.06$	105	0.91	5.2	8.0
E	230 (fixed)	$2610 \pm 120$	$0.78 \pm 0.07$	60	1.09	9.5	26.5
F	230 (fixed)	$2990 \pm 140$	$0.79 \pm 0.10$	53	0.92	4.7	4.0

column densities. However, if smaller regions are considered, the strong correlation between the two fit parameters  $C_{Fg}$  and  $C_{Bg}$  requires to fix one of them. If we only consider regions where no significant amounts of neutral gas inside the LHB is detected the foreground count rate can be fixed to the value derived by the fit for the diffuse galactic H I.

- The distant X-ray emitting plasma ( $T = 10^{6.3}$  K) is roughly 12 times more luminous in the  $\frac{1}{4}$  keV band than the Local Hot Bubble in the region of the Draco nebula. We derive a lower background-to-foreground ratio ( $\simeq 7$ ), well in agreement with similar analyses of Snowden et al. (1991) and Kerp (1994), if the plasma temperature of the distant component is about  $10^{6.0}$  K instead of  $10^{6.3}$  K. We did not find variations larger than 15% in the X-ray intensity behind the Draco nebula on scales of about one degree.
- The emission measure of the LHB component is  $EM_{LHB} = 0.0011$  cm $^{-6}$  pc if a plasma temperature of  $10^{5.85}$  K is assumed. For the distant component ( $T = 10^{6.3}$  K) we get  $EM_{dist} = 0.0055$  cm $^{-6}$  pc. The ratio of the emission measures is roughly  $EM_{LHB}/EM_{dist} = 0.2$  which is in agreement with the result of Kerp (1994) whereas our absolute values are lower by about a factor of 2.
- The most prominent X-ray shadows are deeper than can be explained by H I alone. We conclude that there is more X-ray absorbing gas than implied by H I. The total absorbing hydrogen column densities at these positions are up to  $3 \cdot 10^{20}$  cm $^{-2}$  larger than the observed H I column densities. Since CO line emission has been found at these positions the detected excess of X-ray absorbing gas can be interpreted as molecular hydrogen, H $_2$ , associated with the Draco nebula.
- We have found a linear relation between the total absorbing column density ( $N(\text{H I, DN}) + 2 N(\text{H}_2) \equiv N(\text{H})$ ) and the IRAS 100  $\mu\text{m}$  intensity of the dust associated with the Draco nebula. We get a FIR-emissivity per hydrogen nucleon of  $I_{100}/N(\text{H}) \equiv a_{100}(\text{H}) = 1.02 \cdot 10^{-20}$  MJy sr $^{-1}$  cm $^2$  for the entire Draco nebula, which is in good agreement with the value of  $1.11 \cdot 10^{-20}$  MJy sr $^{-1}$  cm $^2$  found by HHM from a comparison of  $I_{100}$ ,  $N(\text{H I})$  and  $W(^{12}\text{CO})$ . The values in the different subregions of the Draco nebula are in the range  $0.88 < a_{100} < 1.07 \cdot 10^{-20}$  MJy sr $^{-1}$  cm $^2$ , i.e. the FIR-emissivity does not show significant deviations from the mean value. The scatter of the ratio  $I_{100}/N(\text{H I})$  is

much larger. This is further evidence that the excess of X-ray absorbing gas found in these regions is due to molecular hydrogen.

- The largest fraction of molecular hydrogen compared to H I is found at the galactic south-west boundary of the Draco nebula (regions A, C and D). Here we also observe the largest CO line intensities. In regions A and D the  $x_{WCO}$  ratio is in the range  $0.44 < x_{WCO} < 0.52 \cdot 10^{20}$  cm $^{-2}$  (K km s $^{-1}$ ) $^{-1}$ . The very low value of  $0.17 \cdot 10^{20}$  cm $^{-2}$  (K km s $^{-1}$ ) $^{-1}$  found in region C requires a larger CO abundance or an enhanced kinetic temperature. This result tends to a scenario developed by HHM: A collision between the Draco nebula and HVCs (or outer parts of the galactic layer) produces shock fronts. This is leading to chemical reactions which enhance the abundance of the CO molecules relative to that of H $_2$  therefore showing a very low  $x_{WCO}$  ratio.
  - One of the key issues of this paper is the determination of the total hydrogen content, the visual extinction and the total mass of the Draco nebula. The mean and the maximum column densities are summarized in Table 2. The mean column densities of hydrogen nuclei of the examined regions are in the range  $0.6 \leq \overline{N(\text{H})} \leq 1.7 \cdot 10^{20}$  cm $^{-2}$ . This corresponds to very low mean values of the visual extinction  $0.03 \text{ mag} \leq \overline{A_V} \leq 0.09 \text{ mag}$  if the standard gas-to-dust ratio of Bohlin et al. (1978) is adopted. The maximum hydrogen column density of  $4.5 \cdot 10^{20}$  cm $^{-2}$  corresponds to visual extinctions of  $A_V(\text{max}) \simeq 0.24 \text{ mag}$ .
- The total gas mass of the absorbing neutral hydrogen in the Draco nebula is about  $750 M_{\odot} D^2 (500 \text{ pc})^{-2}$  including a molecular mass of approximately  $150 M_{\odot} D^2 (500 \text{ pc})^{-2}$ , i.e. about 20%. The average molecular mass fractions range from 50% in region A, about 35% in regions C and D down to zero in region F.

*Acknowledgements.* We thank Bart Wakker for providing the scanning corrected IRAS 100  $\mu\text{m}$  map, Wolfgang Hirth and Jürgen Kerp for valuable discussions and Luzian Velden for providing his “Non-linear least square fit routine”. P.M. has been supported by the Graduiertenförderung des Landes Nordrhein-Westfalen (GrFG NW) and by the DARA under project No. 50 OR 9402 2.

## References

- Aschenbach B., 1988, *Appl. Opt.* 27, 1404
- Bloemen J.B.G.M., Deul E.R., Thaddeus P., 1990, *A&A* 233, 437
- Bohlin R. C., Savage B.D., Drake J.F., 1978, *ApJ* 224, 132
- Boulanger F., Péroul M., 1988, *ApJ* 330, 964
- Burrows D.N., Mendenhall J.A. 1991, *Nat* 351, 629
- Crudace R., Paresce F., Bowyer S., Lampton M., 1974, *ApJ* 187, 497
- Denne D.R., 1970, *J. of Phys. D* 3, 1392
- de Vries C.P., Heithausen A., Thaddeus P., 1987, *ApJ* 319, 723
- Hasinger G., Burg R., Giacconi R., Hartner G., et al., 1993, *A&A* 275, 1
- Haud U., 1993, Gaussian Decomposition by a modified Levenberg-Marquardt method, Universität Bonn
- Heiles C., 1984, *ApJS* 55, 585
- Heithausen A., Mebold U., 1989, *A&A* 214, 347
- Heithausen A., Thaddeus P., 1990, *ApJ* 353, L49
- Henke B.L., Lee P., Tanaka T.J., Shimabukuro R.L., Fujikawa B.K., 1982, *Atomic Data and Nucl. Data Tables* 27, 1
- Herbstmeier U., 1990, PhD Thesis, Universität Bonn
- Herbstmeier U., Heithausen A., Mebold U., 1993, *A&A* 272, 514 (HHM)
- Herbstmeier U., Mebold U., Snowden S.L., et al., 1995, *A&A* 298, 606
- Herbstmeier U., Kalberla P.M.W., Mebold U., et al., 1996, *A&AS* 117, 497
- Hirth W., Mebold U., Dahlem M., Müller P., 1991, *Ap&SS* 186, 211
- Kalberla P.M.W., Mebold U., Reich W., 1980, *A&A* 82, 275
- Kalberla P.M.W., Mebold U., Reif K., 1982, *A&A* 106, 190
- Kerp J., 1994, *A&A* 289, 357
- Kerp J., Herbstmeier U., Mebold U., 1993, *A&A* 268, L21
- Kerp J., Lesch H., Mack, K.-H., 1994, *A&A* 286, L13
- Kutner M.L., Leung C.M., 1985, *ApJ* 291, 188
- Lampton M., Margon B., Bowyer S., 1976, *ApJ* 208, 177
- Lilienthal D., Wennmacher A., Herbstmeier U., Mebold U., 1991, *A&A* 250, 150
- Lockman J.F., Jahoda K., McCammon D., 1986, *ApJ* 302, 432
- Maloney P., Black J.H., 1988, *ApJ* 325, 389
- Mebold U., Cernicharo J., Velden L., et al., 1985, *A&A* 151, 427
- Mebold U., Heithausen A., Reif K., 1987, *A&A* 180, 213
- Mebold U., Herbstmeier U., Kalberla P.M.W., Souvatzis I., 1989, Molecules at the Interface of an HVC and a High-z HI Filament, in: Tenorio-Tagle G., Moles M., Melnick J. (eds.) *Proc. IAU Coll. 120, Structure and Dynamics of the Interstellar medium, Lecture Notes in Physics, Vol. 350, Springer, Berlin, p. 424*
- Meyerdierks H., Brouillet N., Mebold U., 1990, *A&A* 230, 172
- Meyerdierks H., Heithausen A. 1996, *A&A*, in press
- Morrison R., McCammon D., 1983, *ApJ* 270, 119
- Odenwald S.F., Rickard L.J., 1987, *ApJ* 318, 702
- Pfeffermann E., Briel U.G., Hippmann H. et al., 1987, in *Proc. of SPIE* 733, 519
- Plucinsky P.P., Snowden S.L., Briel U.G., Hasinger G., Pfeffermann E., 1993, *ApJ* 418, 519
- Raymond J.C., Smith B.W., 1977, *ApJS* 35, 419
- Reynolds R.J., 1993, The warm ionized medium, in: Holt S.S., Verter F. (eds.), *Back to the Galaxy, Proc. 3<sup>rd</sup> October Astroph. Conf. in Maryland, American Institute of Physics, Conf. Proc. Vol. 278, p.156*
- Rohlf, R., 1986, Diploma Thesis, Universität Bonn
- Snowden S.L., Freyberg M.J., 1993, *ApJ* 404, 403
- Snowden S.L., Schmitt J.H.M.M., 1990, *Ap&SS* 171, 207
- Snowden S.L., Cox D.P., McCammon D., Sanders W.T., 1990, *ApJ* 354, 211
- Snowden S.L., Mebold U., Hirth W., Herbstmeier U., Schmitt J.H.M.M., 1991, *Sci* 252, 1529
- Snowden S.L., Plucinsky P.P., Briel U., Hasinger G., Pfeffermann E., 1992, *ApJ* 393, 819
- Snowden S.L., McCammon D., Burrows D.N., Mendenhall J.A., 1994a, *ApJ* 424, 714
- Snowden S.L., Hasinger G., Jahoda K., et al., 1994b, *ApJ* 430, 601
- Snowden S.L., Freyberg M.J., Plucinsky P.P., et al., 1995, *ApJ* 454, 643
- Snowden S.L., Egger R., Freyberg M.J., et al., 1997, *ApJ* submitted
- Strong A.W., Bloemen J.B.G.M., Dame T.M., et al., 1988, *A&A* 207, 1
- Trümper J., 1983, *Adv. Space Res.* 2, 241
- Trümper J., 1992, *QJRAS*, 33, 165
- van Albada G.D., Baud B., Boulanger F., et al., 1984, Internal Report. Space Research Laboratory, Groningen
- Voges W., 1992, in *Proc. Satell. Symp. 3, Space Science with Particular Emphasis on High Energy Astrophysics*, ed. T.D. Guyenne & J.J. Hunt (Noordwijk:ESA), 9
- Voges W., et al., 1992, in *Proc. Satell. Symp. 3, Space Science with Particular Emphasis on High Energy Astrophysics*, 223
- Wakker B.P., 1991, *A&A* 250, 499
- Wennmacher A., 1994, PhD Thesis, Universität Bonn